

Dynamic alterations in the central glutamatergic status following food and glucose intake: *in vivo* multimodal assessments in humans and animal models

Journal of Cerebral Blood Flow & Metabolism
2021, Vol. 41(11) 2928–2943
© The Author(s) 2021



Article reuse guidelines:
sagepub.com/journals-permissions
DOI: 10.1177/0271678X211004150
journals.sagepub.com/home/jcbfm



Manabu Kubota^{1,2} , Yasuyuki Kimura^{1,3} ,
Masafumi Shimojo¹, Yuhei Takado¹, Joao MN Duarte^{4,5},
Hiroyuki Takuwa¹, Chie Seki¹, Hitoshi Shimada¹,
Hitoshi Shinotoh¹, Keisuke Takahata¹, Soichiro Kitamura^{1,6},
Sho Moriguchi¹, Kenji Tagai¹, Takayuki Obata⁷ ,
Jin Nakahara⁸, Yutaka Tomita^{8,9}, Masaki Tokunaga¹,
Jun Maeda¹, Kazunori Kawamura¹⁰, Ming-Rong Zhang¹⁰,
Masanori Ichise¹, Tetsuya Suhara¹ and Makoto Higuchi¹

Abstract

Fluctuations of neuronal activities in the brain may underlie relatively slow components of neurofunctional alterations, which can be modulated by food intake and related systemic metabolic statuses. Glutamatergic neurotransmission plays a major role in the regulation of excitatory tones in the central nervous system, although just how dietary elements contribute to the tuning of this system remains elusive. Here, we provide the first demonstration by bimodal positron emission tomography (PET) and magnetic resonance spectroscopy (MRS) that metabotropic glutamate receptor subtype 5 (mGluR5) ligand binding and glutamate levels in human brains are dynamically altered in a manner dependent on food intake and consequent changes in plasma glucose levels. The brain-wide modulations of central mGluR5 ligand binding and glutamate levels and profound neuronal activations following systemic glucose administration were further proven by PET, MRS, and intravital two-photon microscopy, respectively, in living rodents. The present findings consistently support the notion that food-associated glucose intake is mechanistically linked to glutamatergic tones in the brain, which are translationally accessible *in vivo* by bimodal PET and MRS measurements in both clinical and non-clinical settings.

¹Department of Functional Brain Imaging, National Institute of Radiological Sciences, National Institutes for Quantum and Radiological Science and Technology, Chiba, Japan

²Department of Psychiatry, Kyoto University Graduate School of Medicine, Kyoto, Japan

³Department of Clinical and Experimental Neuroimaging, Center for Development of Advanced Medicine for Dementia, National Center for Geriatrics and Gerontology, Obu, Japan

⁴Department of Experimental Medical Science, Faculty of Medicine, Lund University, Lund, Sweden

⁵Wallenberg Centre for Molecular Medicine, Lund University, Lund, Sweden

⁶Department of Psychiatry, Nara Medical University, Nara, Japan

⁷Department of Molecular Imaging and Theranostics, National Institute of Radiological Sciences, National Institutes for Quantum and Radiological Science and Technology, Chiba, Japan

⁸Department of Neurology, Keio University School of Medicine, Tokyo, Japan

⁹Tomita Hospital, Aichi, Japan

¹⁰Department of Radiopharmaceutics Development, National Institute of Radiological Sciences, National Institutes for Quantum and Radiological Science and Technology, Chiba, Japan

Corresponding authors:

Manabu Kubota, Department of Functional Brain Imaging, National Institute of Radiological Sciences, National Institutes for Quantum and Radiological Science and Technology, 4-9-1 Anagawa, Inage-ku, Chiba 263-8555, Japan.

Emails: kubota.manabu@qst.go.jp; m_kubota@kuhp.kyoto-u.ac.jp

Makoto Higuchi, Department of Functional Brain Imaging, National Institute of Radiological Sciences, National Institutes for Quantum and Radiological Science and Technology, 4-9-1 Anagawa, Inage-ku, Chiba 263-8555, Japan

Email: higuchi.makoto@qst.go.jp

Keywords

glucose, glutamate, metabotropic glutamate receptor subtype 5, positron emission tomography, magnetic resonance spectroscopy

Received 10 December 2020; Revised 24 February 2021; Accepted 28 February 2021

Introduction

Tones of excitatory versus inhibitory neuronal activities, often referred to as excitation-inhibition (E-I) balances,¹ determine the efficiency of neural coding, underlying relatively slow transitions of brain functions as exemplified by attention, wakefulness, sense of fatigue, and susceptibility to stress.^{2,3} The global E-I balance may fluctuate as a consequence of systemic changes in metabolic tones induced by food intake, while little is known regarding mechanistic links between specific dietary components and tonic neuronal activities in the brain.

Glutamate and gamma-aminobutyric acid (GABA) are metabolically converted from glutamine in excitatory and inhibitory pre-synapses, respectively,⁴ and astrocytes supply glutamine by generating it from glutamate.^{5–8} As *de novo* synthesis of glutamate results from the tricarboxylic acid (TCA) cycle following glycolysis in astrocytes, utilization of dietary glucose may be pivotally involved in the modulation of synaptic tones via energy-synthesizing processes in these cells. Profound changes in tonic neuronal activities under glycopenic conditions in the brain are likely to induce fatigue and lack of concentration as represented by manifestations in Addison's disease,⁹ and swings of brain glucose levels related to daily life activities including food intake in healthy circumstances are thought to affect the functionality of neural networks at a lower magnitude.

Despite these potential impacts of glucose and other dietary metabolites on the E-I shift of constitutive neuronal activities, the availability of technologies for monitoring glutamatergic and GABAergic statuses in the living brain has been limited. Magnetic resonance spectroscopy (MRS) offers a means to noninvasively measure relatively abundant metabolites, including glutamine, glutamate, and GABA, in tissues.^{10–13} Components of glutamate neurotransmission, such as metabotropic glutamate receptors subtype 1 and subtype 5 (mGluR5), have been visualized and quantified by *in vivo* positron emission tomography (PET) with specific radioligands.^{14–16} Notably, mGluR5 radioligand binding assessed by PET has recently been reported to fluctuate in a single subject within one day,^{17,18} implying the vulnerability of interactions

between mGluR5 and its exogenous ligand to synaptic glutamate levels modified by physiological processes. The excitatory neuromodulation, coupled with daily life events, would be clarified by examining coupled or uncoupled changes in mGluR5 and glutamate by bimodal PET and MRS assays.

This experimental paradigm was applied to the current work in order to investigate whether dietary nutrients and their metabolites trigger glutamatergic tones in the brain following regular food intake.

Materials and methods

Human experiments

Subjects. Sixteen healthy male volunteers (26 ± 5 years) were enrolled in this study. None had current or past psychiatric disorders, substance abuse, organic brain disease, or organic diseases such as diabetes based on their medical history and MR imaging (MRI) of the brain. They underwent two mGluR5 PET scans with a specific radioligand, (*E*)-[¹¹C]ABP688,¹⁹ and two MRS scans on the same day. They were assigned to either with ($n = 5$) or without ($n = 11$) food intake between the two PET scans. This human experiment was approved by the Radiation Drug Safety Committee and the Institutional Review Board of the National Institute of Radiological Sciences, Japan, and was carried out in accordance with the Code of Ethics of the World Medical Association. After a complete description of the study, written informed consent was obtained from all participants. The study was registered with the University Hospital Medical Information Network Clinical Trials Registry (UMIN000014978).

PET procedures and kinetic analysis. All participants underwent two PET scans (PET-Scan 1 at around 11:00 and PET-Scan 2 at around 14:00) on the same day. Among all subjects, arterial blood was sampled during the PET scan to obtain arterial input functions for 11 subjects, except for 5 assigned to the no-food intake condition.

For subjects assigned to the food intake condition, blood levels of glucose, insulin, triglyceride, leptin, and

active ghrelin were measured at a commercial laboratory twice, shortly before the initiation of each PET scan. Among the 11 subjects assigned to the no-food intake condition, 5 subjects underwent PET imaging without arterial sampling to examine a potential stress effect related to the arterial cannulation.

For more details about PET procedures, experimental design, experimental conditions and data analysis, see Supplementary Methods.

PET kinetic analysis. For subjects with arterial data, the total distribution volume (V_T) was estimated by Logan graphical plot²⁰ using the radiometabolite-corrected plasma input function in each region of interest (ROI: frontal, temporal, parietal, occipital, anterior cingulate, posterior cingulate and insular cortices, and thalamus, caudate, putamen, amygdala, hippocampus and cerebellar cortex). The brain blood volume contribution was fixed at 5%.

MRI/MRS imaging procedures. All MRI and MRS scans were performed with a 3-T MRI scanner (MAGNETOM Verio, Siemens, Germany). Structural T1-weighted images were acquired for all subjects. The same-day two MRS scans (MRS-Scan 1 and MRS-Scan 2) were conducted for all subjects before PET-Scan 1 and after PET-Scan 2, respectively. A T2-weighted image was acquired prior to each MRS scan and used for the positioning of a ROI ($20 \times 20 \times 25 \text{ mm}^3$) in the right posterior insula. For parameters of T1- and T2-weighted images, see Supplementary Methods. We selected the insula because of its involvement in glucose metabolism^{21,22} and food-associated processing,^{23,24} and also in the processing of the systemic physiological condition.²⁵ MRS was performed using a point-resolved spectroscopic localization sequence (PRESS) with WET water suppression²⁶ with the following parameters: TE/TR, 30/2000 ms; bandwidth, 2000 Hz; number of averages, 64; vector size, 1024.

MRS quantification. MRS data processing was performed with LCModel (ver. 6.2-1G, Stephen Provencher Inc., Oakville, Ontario, Canada). The “basis-set” of model spectra for the Siemens 3T PRESS sequence in the LCModel package was used as reference, to facilitate separation of the spectra using linear combinations of individual metabolite spectra. In the current study, the glutamate level was assessed (we used the level of “glutamate” instead of “glutamate plus glutamine [Glx]” in all our MRS analyses). Data reliability was ensured by excluding any data associated with a signal-to-noise ratio (ratio of the spectrum maximum minus the baseline divided by twice the root mean square of the residual) of less than 8 or a percentage standard

deviation value of more than 30 (in fact, the values were 21 or less for all data), similar to previous studies.^{27,28}

Statistical analysis. All the statistical analyses in our current study were conducted with SPSS 23.0 (SPSS Inc., Chicago, IL, USA), and the statistical significance threshold was defined as $p < 0.05$ (two-tailed), unless otherwise specified. Normal distribution of each variable (in our human and also animal experiments) was confirmed by the Kolmogorov-Smirnov test for significance.

We firstly conducted independent-sample t-tests to examine group differences (between the groups with and without food intake) in V_T in the cerebral ROI and glutamate levels in the right posterior insula at the 1st PET and MRS scans, respectively. Next, in the groups with and without food intake conditions separately, repeated-measures analysis of variance (rm-ANOVA) was used to examine the effect of a scan (1st or 2nd) on V_T and on glutamate levels. A within-subject variable was a scan, and a dependent variable was either V_T in the cerebral ROI or glutamate level in the right posterior insula for each scan. In case significant scan effects were found on V_T or glutamate levels, we performed correlation analyses between V_T in the right posterior insular ROI (defined using a FreeSurfer atlas²⁹) and the glutamate level in the right posterior insula (for the 1st scan, and for their % changes between the 1st and 2nd scans) to investigate associations between regional mGluR5 binding and glutamate levels.

To investigate whether blood levels of glucose, insulin, triglyceride, leptin, and active ghrelin were changed between the 1st and 2nd scans, rm-ANOVA was used for the food intake condition group. A within-subject variable was a scan, and a dependent variable was the blood level of either glucose, insulin, triglyceride, leptin, or active ghrelin for each scan.

Animal experiments

To corroborate our findings in humans, we conducted animal experiments with PET (Experiment 1,2), MRS (Experiment 3), *in vivo* two-photon calcium imaging (Experiment 4), *ex-vivo* biochemical (Experiment 5), and *in-vitro* culture (Experiment 6) assays.

Experiments 1, 2, 4, 5, and 6 were conducted at the National Institute of Radiological Sciences, Chiba, Japan, in accordance with National Research Council's Guide for the Care and Use of Laboratory Animals and the institutional guidelines. The experimental procedures related to the animals and their care were approved by the Animal Ethics Committee

of the National Institutes for Quantum and Radiological Science and Technology.

Experiment 3 was conducted at the Laboratory of Functional and Metabolic Imaging, Lausanne, Switzerland. The experiments were conducted according to European Union directive 2010/63/EU and Swiss legislation on animal experimentation, and all procedures were approved by the local ethics committee (EXPANIM-SCAV, Switzerland).

All the animal experiments were reported following the ARRIVE (Animal Research: Reporting in Vivo Experiments) guidelines.

Experiments 1 and 2: mGluR5 PET

Preparation of animals. Male Sprague-Dawley rats (Japan SLC, Japan) (weighing 380 ± 63 g for Experiment 1, and 316 ± 40 g for Experiment 2) were housed two or three per cage at a constant room temperature (25°C) under a 12:12 h light-dark cycle (light from 07:00 to 19:00) for 2–4 weeks. The rats underwent operation with an acrylic cap applied to the top of their skull in order to fixate their heads. An anatomical template of rat brain consisting of axial T1-weighted MR images was obtained with 3-T Philips Intera (Philips Electronic) by means of a three-dimensional spin-echo sequence.

PET protocol. *Experiment 1.* Six rats underwent two PET scans (Scan 1 and Scan 2) on the same day with feeding between the scans (feeding condition), and received another set of two serial scans on a different day without feeding between the scans (non-feeding condition), with an interval of 7 days or longer. All PET scans were carried out under food deprivation from the previous night. Starting times for Scan 1 and Scan 2 were either 10:00 and 14:00, or 11:00 and 15:00, respectively. In the feeding condition, rats received oral dosage of 1 g/kg body weight, DietGel® 76A (ClearH₂O®, ME, USA; Table S1) via feeding tube between the two scans. Sham feeding was not conducted on the day of the non-feeding condition. Scan protocols were pursuant to clinical trials.

Experiment 2. Four rats underwent two PET scans (control condition and glucose-load condition) on different days, with an interval of 7 days. Each scan was begun at 12:00 under conscious condition. For the glucose-load condition, rats received oral dosage of 2 g/kg glucose 30 minutes prior to the PET scan.

For details of PET measurements and kinetic analysis, see Supplementary Methods. Since, unlike humans, the rat cerebellum is devoid of mGluR5, we directly quantified radioligand binding as binding

potential, which is a specific versus non-displaceable radioactivity uptake (BP_{ND}).

Statistical analysis. *Experiment 1.* We performed rm-ANOVA to examine whether the presence or absence of feeding between the two same-day scans affects mGluR5 binding. A within-subject variable was the condition (feeding or non-feeding). A dependent variable was the % change in BP_{ND} in the cerebral ROI, as calculated by $100 \times ([BP_{\text{ND}} \text{ at Scan 2}] - [BP_{\text{ND}} \text{ at Scan 1}]) / (BP_{\text{ND}} \text{ at Scan 1})$, for both feeding and non-feeding conditions. In case a significant effect of condition was found, BP_{ND} in each ROI at each scan was further investigated.

Experiment 2. We performed rm-ANOVA to examine the effect of condition (control or glucose-loads) on mGluR5 binding. A within-subject variable was the condition. A dependent variable was BP_{ND} in the cerebral ROI. In case a significant effect of condition was found, BP_{ND} in each ROI for both conditions was further investigated.

Experiment 3: MRS. Six male Sprague-Dawley rats (266–290 g, obtained from Charles River Laboratoires, France) underwent MRS scans under 1.5% isoflurane anesthesia as previously described.³⁰ Before MRS, polyethylene catheters were inserted into a femoral artery for monitoring blood gases, arterial blood pressure, and glucose and lactate levels, and into a femoral vein for infusion of 20% D-glucose (w/v) in saline. During MRS acquisition, glucose was given as a bolus and then continuously infused at a rate adjusted based on concomitantly measured arterial plasma glucose levels to maintain a stable level.

MRS was performed with a Direct Drive spectrometer (Agilent, Palo Alto, CA, USA) interfaced to an actively shielded 9.4 T magnet with a 31-cm horizontal bore (Magnex Scientific, Abingdon, UK) using a home-built 12-mm ¹H quadrature surface coil. The rat brain was positioned in the isocenter of the magnet, and fast-spin-echo images were acquired to identify anatomical landmarks and place ROIs in the cortex and hippocampus. For the MRS data acquisition, shimming was performed with FAST(EST)MAP, and ¹H MRS spectra were acquired from a ROI size of 120 μL using SPECIAL with VAPOR water suppression³¹ and analyzed using LCModel with a macromolecule spectrum in the database.^{30,31} In the current study, glucose, glutamate, and GABA levels in the brain were assessed.

Statistical analysis. Linear mixed effect models were applied using the “nlme” package (version 3.1-118)

equipped with R (R Foundation for Statistical Computing, Vienna, Austria) to examine the effects of time on plasma glucose levels, and the levels of glucose, glutamate, and GABA in the brain. A fixed effect was time. A random effect was individual rat ID. A dependent variable was the plasma glucose level, or glucose, glutamate, or GABA level in the brain. Additionally, we compared whether glucose and glutamate levels in the brain differ between the beginning of glucose infusion and 120 min later by paired t-tests.

Experiment 4: In vivo two-photon calcium imaging. A recombinant adeno associated virus (AAV) was produced in HEK293T cells by polyethylenimine mediated co-transfection of AAV transfer plasmid encoding GCaMP6s³² with rat synapsin promoter and serotype DJ packaging plasmids, pHelper and pRC-DJ (Cell Biolabs Inc.). AAV particles were purified with HiTrap heparin column (GE Healthcare) and virus titer was determined by AAVpro[®] Titration kit (for Real Time PCR) ver2 (TaKaRa) as described previously.³³

A total of 12 male C57BL/6 J mice (20–30 g, 7–11 weeks; Japan SLC, Inc., Hamamatsu) were used in experiments with glucose (2 g/kg; n=6) and saline injection (n=6). For the surgical procedure, the animals were anesthetized with a mixture of air, oxygen, and isoflurane (3–4% for induction and 2% for surgery) via a facemask, and a cranial window (3–4 mm in diameter) was attached over the left somatosensory cortex, centered at 1.8 mm caudal and 2.5 mm lateral from the bregma, according to the ‘Seylaz-Tomita method’.³⁴ AAV-Syn-GCaMP6s was injected into cortical parenchyma during this procedure. A custom plastic plate was affixed to the skull with a 7-mm-diameter hole centered over the cranial window. Two-photon imaging was performed in awake mice using our hand-made fixation apparatus, as previously reported.³⁵ Each awake mouse was placed on a custom-made apparatus, and real-time imaging was conducted by wide field-of-view type two-photon laser scanning microscopy (Multiphoton Mesoscope, THORLABS, NJ, USA). Excitation wavelength of 900 nm (commercial laser oscillator) was used for GCaMP6s, and an emission signal was separated by beam splitter (560/10 nm) and detected with a band-pass filter (525/50 nm). Visual field size of the image was 2000 $\mu\text{m} \times 2000 \mu\text{m}$, and in-plane pixel size was 1 μm . Temporal resolution was 5 Hz for 120 s (600 frames/trial). Images were acquired before and 15, 30, 60, 90 and 120 min after injection of glucose or saline (i.p.).

Image analysis of two-photon calcium imaging was performed using Matlab (MathWorks, MA, USA). First, motion correction was performed using

NoRMCorre. The images for all time points were then divided by the first image, and the images of signal change rate were obtained. ROIs were manually drawn on the image obtained by maximum intensity projection (MIP) processing for images for 12 min (120 seconds \times 6 trials). The time-dependent change in average luminance value was then obtained for each ROI.

For statistical analysis, we conducted two-way ANOVA to examine the effects of group (groups of glucose or saline injection), time, and their interaction on neuronal firing frequencies. In case significant effects were found, we performed post-hoc Tukey-Kramer tests for each group to examine neuronal frequency differences between each time point (15, 30, 60, 90 or 120 min) and the time of the injection (0 min). In addition, we examined neuronal frequency differences between these groups at each time point.

Experiment 5: Immunoblot analysis of rat brain tissue. 8–10-week-old male Sprague-Dawley rats (weighing 308 ± 53 g; n=13) received oral administration of either normal saline (n=7) or glucose (2g/kg, oral; n=6) 45 min before being sacrificed by cervical dislocation. Brain tissues were quickly removed, sliced, and lysed in buffer containing 20 mmol/L Tris-HCl, pH7.5, 150 mmol/L NaCl, 1 mmol/L EDTA, 1% Triton X-100, 0.1% SDS, protease inhibitor and phosphatase inhibitor cocktails by sonication. The protein extract was then cleared by centrifugation (15,000 g, 10 min) and the supernatant was collected as total lysate. To determine the total protein levels of mGluR5, the lysate was separated by SDS-PAGE with 5–20% Tris-glycine gel (Nacalai Inc) followed by conventional immunoblot analysis with polyclonal anti-mGluR5 antibody (Millipore, AB5675) or anti- β actin antibody (Sigma, A1978) and HRP conjugated secondary antibodies (Jackson IR lab). ECL-mediated chemiluminescent signal was captured by Amersham Imager 600 (GE Healthcare), and signal intensity was quantified by Image J software. We conducted independent-samples t-tests to examine group differences (saline or glucose-load) in total mGluR5 protein levels (monomer and dimer), and also to examine group differences (saline or glucose-load) in total mGluR5 protein levels (monomer and dimer).

Experiment 6: Glutamate concentration in neuronal culture medium. To investigate whether glucose stimulates glutamate release from neuronal cells, we incubated primary neuronal culture in conditioned medium containing various concentrations of glucose and measured the extracellular levels of glutamate. For details of neuronal culture, see Supplementary Methods.

Statistical analysis. We conducted ANOVA to compare glutamate concentrations among four conditions: control, glucose 50 mmol/L, glucose 250 mmol/L, and KCl conditions. In case a significant effect of condition was found, post-hoc analysis was conducted to examine the difference in glutamate concentration for each condition.

Results

Human experiments

Changes in central mGluR5 ligand binding and glutamate levels following food intake. Between the groups with and without food intake, there were no significant differences at the 1st scan in either radioligand binding to mGluR5, as assessed by estimating V_T ($t = -1.80$, $p = 0.11$), or glutamate levels ($t = -0.04$, $p = 0.97$) (Table 1). V_T was increased across extensive brain areas (average change, 28.8%; $p = 0.009$, $F = 21.87$, degree of freedom [DOF] = 4 by rm-ANOVA), and glutamate levels in the right posterior insula were elevated (average change, 9.9%; $p = 0.019$, $F = 14.69$, DOF = 4 by rm-ANOVA) following food intake (Figures 1 and 2(a) and (b), Table 1, Table S2). By contrast, subjects without inter-session food intake exhibited declined V_T values (average change, -19.7% ; $p = 0.016$, $F = 12.64$, DOF = 5 by rm-ANOVA) and glutamate levels (average change, -8.5% ; $p = 0.014$, $F = 9.14$, DOF = 9 by rm-ANOVA) throughout the corresponding target regions in the 2nd scans (Figures 1 and 2(a) and (b), Table 1, Table S2). The radioligand availability for the transfer

from blood to the brain, as assessed by the free fraction in plasma, did not significantly differ between the scans: the average values for each group changed in the same direction as the change in V_T between scans, but the degree of the free fraction change was much smaller than the V_T change across conditions (Supplementary Methods, Result S1). The mGluR5 binding change was not associated with stress-related hormonal change, which could be caused by the arterial cannulation in our experiment (Result S2, Figure S1, Table S3).

Between the two scans, we observed a significant positive correlation between changes of regional V_T and of glutamate levels in the right posterior insula (Pearson's $r = 0.67$, $p = 0.036$; Figure 2(c)), while their correlation at the 1st scan remained at a trend level ($r = 0.42$, $p = 0.20$, Figure 2(c)).

Changes in blood measures following food intake. Plasma glucose ($p = 0.018$, $t = -3.89$, DOF = 4) and serum insulin ($p = 0.039$, $t = -3.04$, DOF = 4) levels under food intake condition were significantly elevated by food intake between the two assaying sessions as examined by paired t-tests ($n = 5$), while other blood measures potentially associated with eating, including triglycerides, leptins, and ghrelin, were not altered between the scans (Table S4). Associations between V_T and blood measures are illustrated in Figure S2.

Animal experiments

Experiment 1: PET (feeding and non-feeding conditions). A significant main effect of condition was found by rm-

Table 1. mGluR5 radioligand binding quantified by total distribution volume (V_T [mL/mm³]), glutamate levels in the 1st and 2nd sessions on the same day, and changes of these parameters between the two sessions in human subjects.

	Food intake condition				No-food intake condition				Difference between conditions	
	n	Mean (S.D.)	Effect of scan		n	Mean (S.D.)	Effect of scan			
			F	p			F	p	t	p
V _T (cerebral ROI)			21.87	0.009*			12.64	0.016*		
PET-scan 1	5	4.07 (0.60)			6	3.47 (0.51)			−1.80	0.11
PET-scan 2	5	5.20 (0.65)			6	2.74 (0.27)				
Change (%)	5	28.85 (17.62)			6	−19.65 (14.37)				
Glutamate (right posterior insula)			14.69	0.019*			9.14	0.014*		
MRS-scan 1	5	0.99 (0.08)			11	0.99 (0.17)			−0.04	0.97
MRS-scan 2	5	1.08 (0.05)			10	0.90 (0.15)				
Change (%)	5	9.94 (6.41)			10	−8.50 (8.76)				

An independent-samples t-test was applied to compare baseline differences in V_T in the cerebral ROI and glutamate levels in the right posterior insula between the groups with and without food intake. In these groups separately, repeated-measures analysis of variance (rm-ANOVA) was applied to examine the effect of a scan (1st or 2nd) on V_T and on glutamate levels.

* $p < 0.05$ by rm-ANOVA.

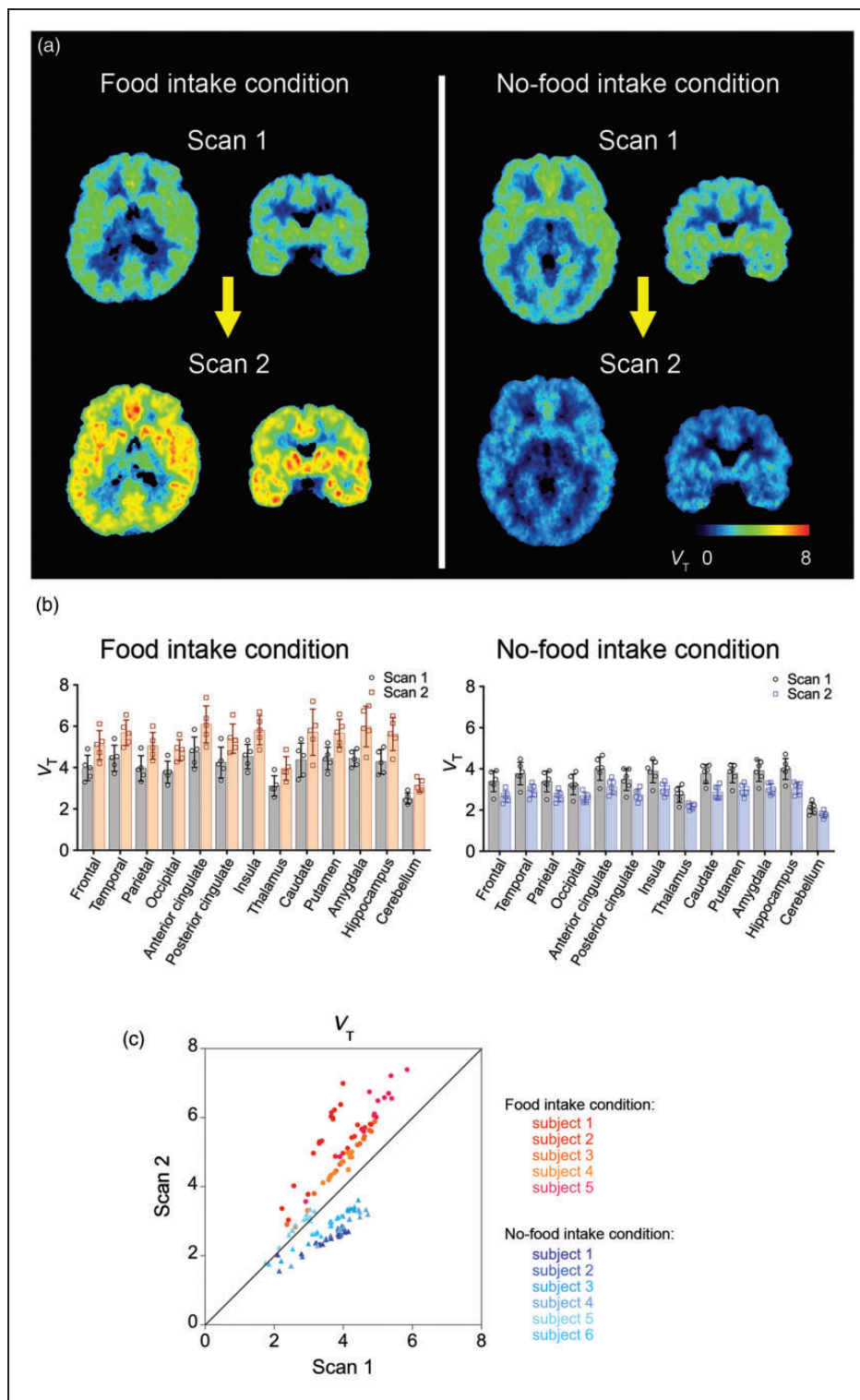


Figure 1. PET images of mGluR5 in human brains acquired with (E)-[11 C]ABP688 on the same day. (a) Representative whole-brain V_T images from the 1st and 2nd PET scans of a subject in the food intake condition (left) and another subject in the no-food intake condition (right). (b) V_T for (E)-[11 C]ABP688 in the 1st and 2nd PET scans across brain regions in the food intake (n = 5) and no-food intake (n = 6) conditions. Error bars represent standard deviation. (c) Scatter plot of V_T for (E)-[11 C]ABP688 in the 2nd PET scan against V_T in the 1st PET scan across brain regions in each subject (red to orange, food intake condition; blue to light-blue, no-food intake condition). V_T , total distribution volume (mL/mm^3).

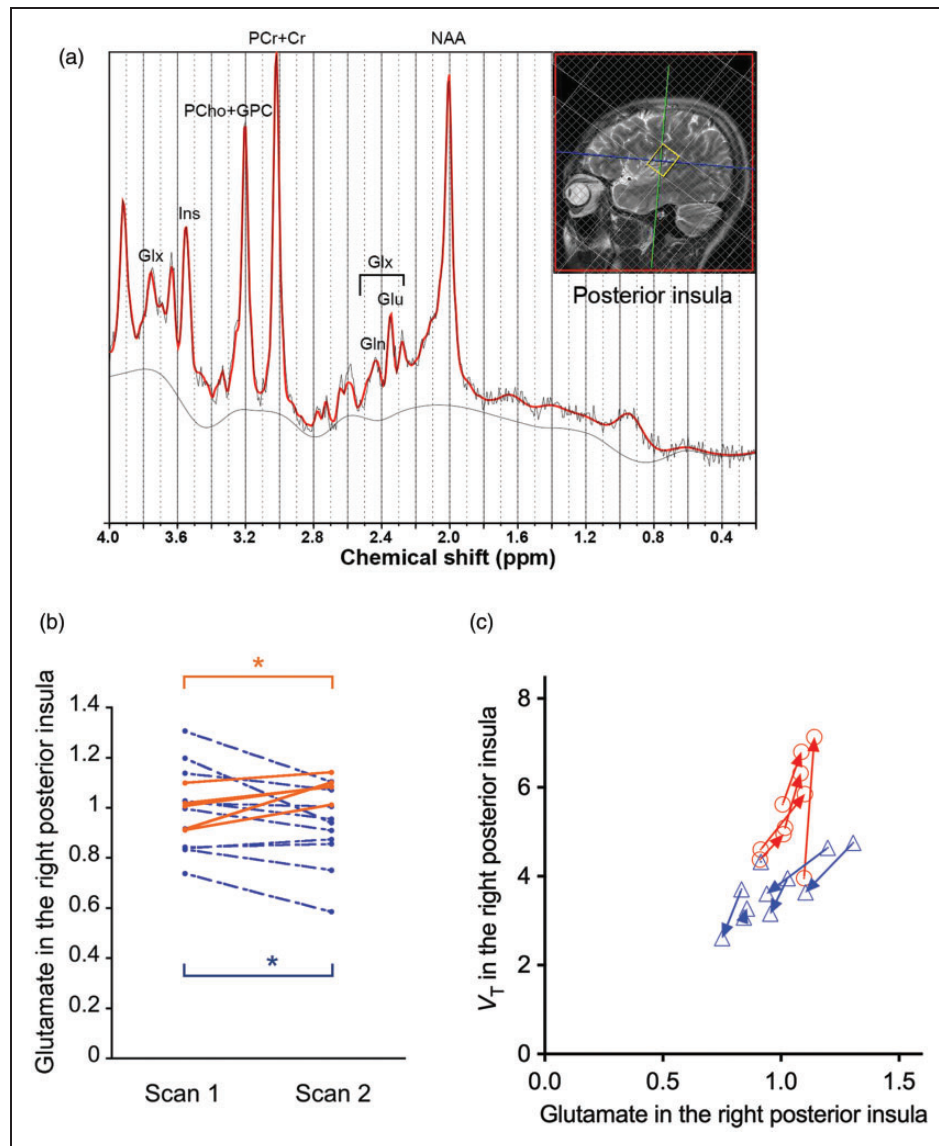


Figure 2. Glutamate levels measured by the two MRS assays, and association of mGluR5 radioligand binding with cerebral glutamate levels in our human experiments. (a) ROI in the right posterior insula used for the MRS experiment, and representative fitting of MRS spectrum to LCModel. (b) Glutamate levels in the right posterior insula in the 1st and 2nd MRS sessions in the groups of food intake (orange, $n = 5$) and no-food intake (blue, $n = 10$) conditions. In each group separately, repeated-measures analysis of variance (rm-ANOVA) was applied to examine the effect of a scan (1st or 2nd) on V_T and on glutamate levels. * $p < 0.05$ by rm-ANOVA. (c) Association between mGluR5 radioligand V_T and glutamate levels in the right posterior insula (21 data sets consisting of 2 scans/subject \times 5 subjects in the food intake condition [orange] and 6 subjects in the no-food intake condition [blue], excluding data from the 2nd scan in one subject due to poor MRS spectrum quality). In panel c, arrows connect data points from the 1st and 2nd scans in the same individual. V_T , total distribution volume (mL/mm^3).

ANOVA ($p = 0.025$, $F = 9.90$, $\text{DOF} = 5$) on BP_{ND} , and the presence and absence of feeding induced an increase (10.1–19.4%) and decrease (2.3–19.5%), respectively, of BP_{ND} in the second PET scan relative to the first scan (Figure 3(a), Table S5). We additionally examined whether BP_{ND} in the cerebral ROI in the 1st scans differs between the days of feeding and non-feeding conditions by paired t-test, and found no significant difference ($t = -1.76$, $p = 0.14$).

Experiment 2: PET (glucose-load). Mean BP_{ND} was increased by 18.2% after a systemic glucose load as compared to a control condition, and rm-ANOVA demonstrated a significant main effect of the condition ($p = 0.004$, $F = 62.29$, $\text{DOF} = 3$) (Figure 3(b), Table S6).

Experiment 3: MRS. Linear mixed effect models showed significant effects of time on plasma glucose levels

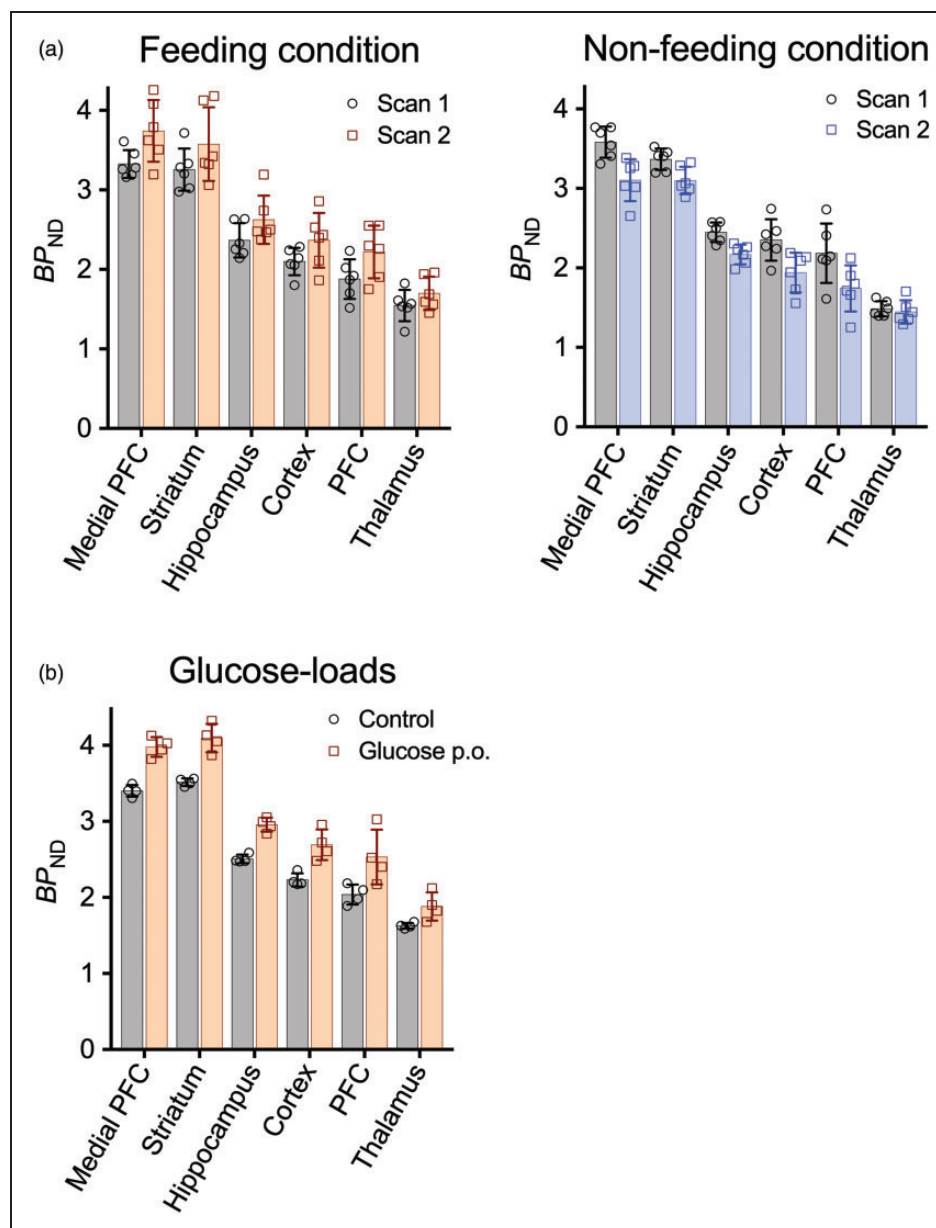


Figure 3. Food- and glucose-related changes of mGluR5 radioligand binding in rat PET experiments. (a) Regional (E)-[¹¹C]ABP688 binding in two serial PET experiments on the same day in the feeding ($n = 6$) and non-feeding ($n = 6$) conditions. (b) Regional (E)-[¹¹C]ABP688 binding in PET experiments with glucose loads ($n = 4$). Error bars represent standard deviation, and dotted lines denote regressions. BP_{ND}, non-displaceable binding potential; PFC, prefrontal cortex.

($p = 0.001$, average 134.8% increase after two hours), and on levels of glucose, glutamate, and GABA in brain ($p < 0.001$ for all). As shown in Figure 4, glucose levels in brain increased during the first 40 min after initiation of glucose infusion, then reaching a plateau, while glutamate levels increased gradually. Infusion of glucose over two hours resulted in significant increases of glucose ($p < 0.001$, $t = -16.51$, $\text{DOF} = 5$) and glutamate ($p = 0.001$, $t = -7.67$, $\text{DOF} = 5$) levels in brain. In the meantime, there was a slight, insignificant increase

of central GABA levels ($p = 0.06$, $t = -2.38$, $\text{DOF} = 5$) concurrently with glucose infusion (Figure 4).

Experiment 4: In vivo two-photon calcium imaging. After injections of glucose, the frequency of spontaneous neuronal activation increased gradually and plateaued at 60 min (Figure 5). There were main effects of treatment group ($p < 0.001$, $F = 43.91$, $\text{DOF} = 25$) and time ($p < 0.001$, $F = 4.64$, $\text{DOF} = 25$), and interaction between group and time ($p < 0.001$, $F = 4.93$,

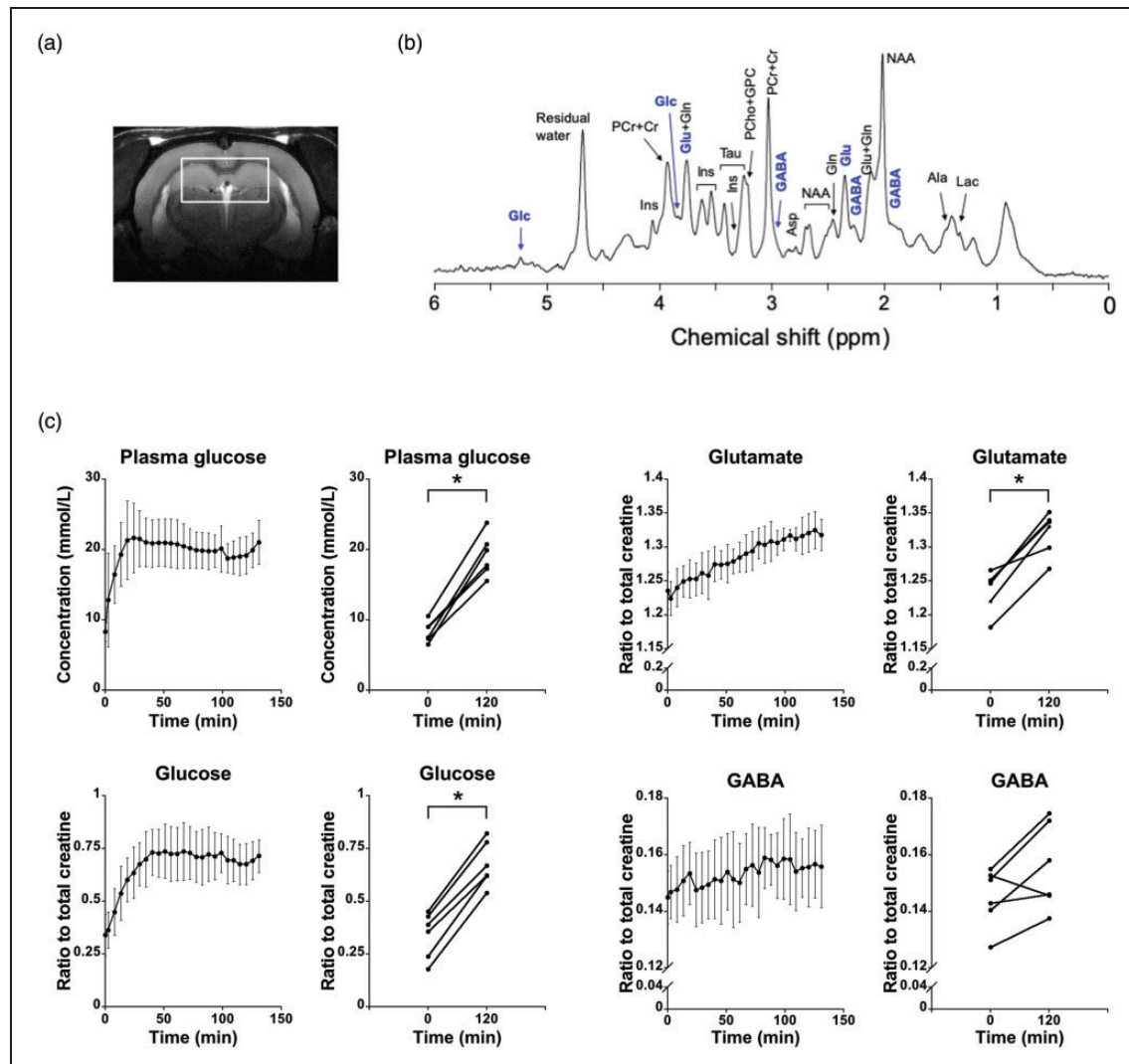


Figure 4. Brain metabolite levels measured by MRS during a glucose clamp in rats under isoflurane anesthesia ($n = 6$). (a) ROI used in the rat MRS experiment. (b) An example of MRS spectrum acquired from the ROI. (c) Levels of plasma glucose, and glucose, glutamate, GABA in the brain after glucose injection. Error bars represent standard deviation. Significant effects of time were found on glucose, glutamate, and GABA levels in the brain ($p < 0.001$ for all). Two hours after glucose infusion, glucose ($p < 0.001$) and glutamate ($p = 0.001$) levels in the brain significantly increased as compared to baseline, while there was a slight, insignificant increase of GABA levels ($p = 0.06$). * $p < 0.05$ as compared to baseline.

DOF = 25) by two-way ANOVA. Neuronal firing frequencies continued at higher levels until 120 min after the injection ($p < 0.001$, $p = 0.0037$, and $p = 0.0025$ at 60, 90, and 120 min, respectively, as compared to the vehicle injection group at the same time points). By contrast, vehicle injection did not change the firing frequency of the same neurons (Figure 5).

Experiment 5: Ex vivo analysis. We found no significant difference in the levels of monomeric ($p = 0.77$) and dimeric ($p = 0.94$) receptor species between the two treatment groups (Figure S3). Hence, altered mGluR5 ligand binding in PET scans after glucose

load could not occur from changes in the total receptor amount.

Experiment 6: Cell culture analyses. A significant effect of condition was found on glutamate concentrations ($p < 0.001$, $F = 19.77$, DOF = 24 by ANOVA; Figure S4). A post-hoc analysis showed that the glutamate concentration in the glucose 250 mmol/L condition was significantly higher compared to the control condition ($p = 0.005$, 33.7% higher on average). There were no significant differences in glutamate concentration between the glucose 250 mmol/L and 50 mmol/L conditions ($p = 0.6$), nor between the glucose

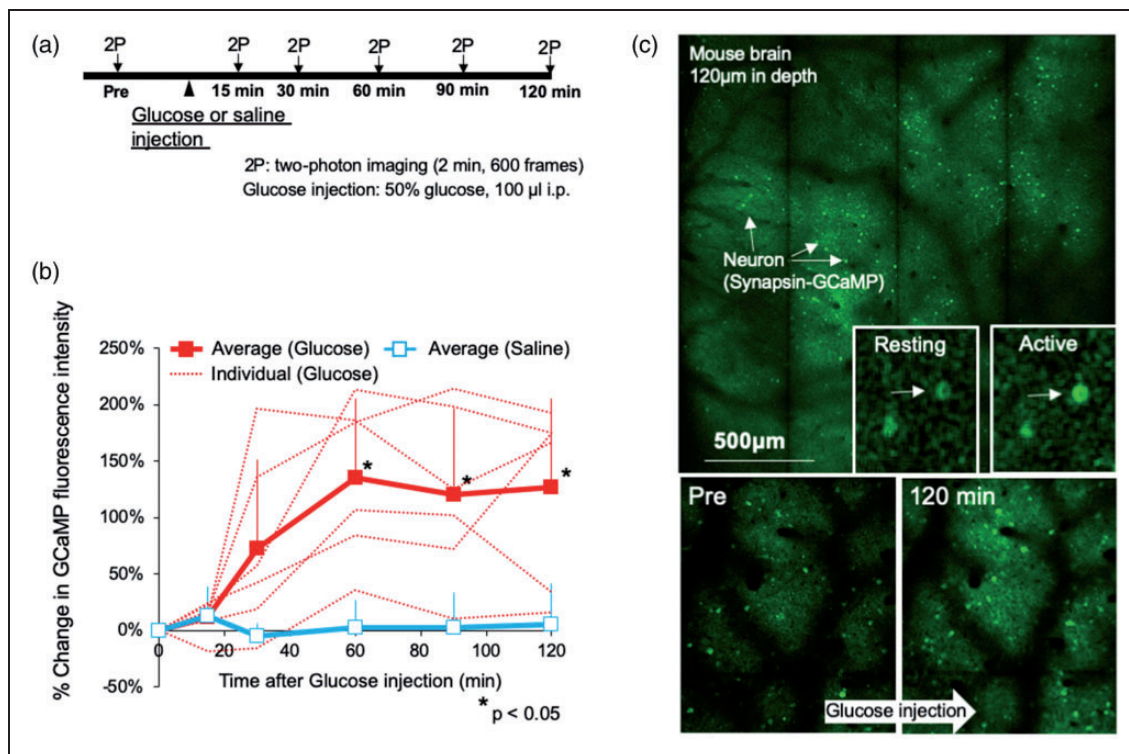


Figure 5. Excitability of neocortical neurons in unanesthetized mice assessed by wide-field two-photon microscopy. (a) Experimental protocol. Two-photon calcium imaging was performed before and 15, 30, 60, 90 and 120 min after injection of glucose ($n = 6$) or saline ($n = 6$) (i.p.). (b) Changes of GCaMP fluorescence intensity in each neuron after glucose or saline injection as % of baseline value. Error bars represent standard deviation. * $p < 0.05$ as compared to baseline. (c) Images obtained by wide-field two-photon excitation microscopy before and 120 min after glucose injection. Arrows show images of neurons obtained with two-photon CaMKII-GCaMP6 imaging. Fluorescence intensity increased during neural activation.

50 mmol/L and control conditions ($p = 0.2$). Glutamate concentration in the KCL condition was also significantly higher compared to the other 3 conditions ($p < 0.032$).

Discussion

With bimodal PET and MRS assays in rodents and humans, we have shown that the intake of dietary nutrients and consequent glucose digestion increase mGluR5 binding and glutamate levels in the brain, whereas the lack of such supplementation drives opposite changes. Alterations in regional mGluR5 radioligand binding positively correlate with altered glutamate levels and reflect their dynamic changes, and there are also intimate links between brain glutamate levels, glucose levels, and plasma glucose levels. Glucose-induced modulations of glutamatergic activity were further supported by our live-cell two-photon microscopic and *in vitro* cell culture assays.

It is particularly noteworthy that our mGluR5 PET data indicate an enhanced glutamate release following a rise of plasma glucose levels, raising the possibility of an increase in the E-I ratio engendered by systemic

glucose intakes. MRS findings in rodents support the robust elevations of cortical glutamate levels in concurrence with modest fluctuations of GABA levels, which are attributable to the accelerated synthesis of these transmitters from glutamine as a consequence of the stimulated glucose-glutamate-glutamine pathway in astrocytes. However, the PET demonstration of concentrated synaptic glutamate molecules implies that the GABA release in inhibitory synapses is unlikely to noticeably alter, since GABA acts on the presynaptic terminals of excitatory synapses, resulting in suppressed glutamate release from these terminals. The glucose-induced activation of excitatory neurons, including neocortical pyramidal cells, was further illustrated by the use of two-photon laser microscopy. In addition, glutamate releases driven by the coordination of neurons and astrocytes were shown by the co-culture experiment, although the results of the neuronal assay should be interpreted as preliminary, because of differences between *in vitro* conditions and the physiological environment.

Numerous reports have documented an altered PET radioligand binding during the physiological and pharmacological neuromodulations. The binding of a

classical PET tracer for D₂ dopamine receptors, [¹¹C] raclopride, is known to be reduced following a surge of synaptic dopamine concentrations, as these exogenous and endogenous ligands compete with each other on the target binding sites.^{36–38} In contrast, radiolabeled spiperone, which has a much higher affinity (dissociation constant, ~0.1 nM³⁹) for D₂ receptors than raclopride (dissociation constant, 2–4 nM⁴⁰), is barely displaced by endogenous dopamine on the target, and its binding was found to be increased by dopaminergic stimulations.³⁹ This change reflects dopamine-induced internalization of the receptors in coated vesicles, involving entrapment of receptor-bound spiperone in these vesicles.³⁹ Similarly, (*E*)-[¹¹C]ABP688, an allosteric ligand for mGluR5, does not compete with glutamate on the receptors, and its binding is accordingly considered to be increased by glutamatergic enhancements and the resulting internalization of mGluR5. Meanwhile, the total amount of mGluR5 in neurons is not likely to change according to glucose availability, in view of our *ex vivo* biochemical measurement in the rat brain.

However, the above explanation is only one of the possibilities, and in our current study we have not proven the underlying mechanism. Therefore, interpretation of our results should be handled with considerable caution, as follows. First, there have also been conflicting results regarding the extent of spiperone's affinity for internalized D₂ receptors.^{41,42} In the case of (*E*)-[¹¹C]ABP688, its accessibility to internalized receptors remains to be elucidated. Second, our results do not directly confirm that glutamate release in the brain leads to internalization of mGluR5. Experiments to measure mGluR5 both on the surface of the cell membrane and in a state of internalization before and after glutamate release will be necessary. Third, for understanding the central mGluR5 function in relation to glutamate, it would be necessary to take into consideration the possibilities that various factors other than the receptor internalization, including inter-individual variability, may influence the mGluR5 status.

The preferential activation of glutamate versus GABA transmissions downstream to the augmented glucose metabolism might be explained by the glutamate release from astrocytes, leading to the excitation of nearby synaptic and extrasynaptic glutamate receptors.⁴³ This mechanism may highlight the role of astrocytes as a modulator of neuronal tones in response to systemic nutrient signaling. Moreover, mGluR5 is expressed in neurons and astrocytes, and glutamate released from presynaptic terminals and astrocytes can activate astrocytic mGluR5, inducing chain reactions of enhanced calcium signaling and release of purines, which act on excitatory presynapses towards sustained glutamate releases from axonal boutons

(Figure 6).⁴⁴ Hence, (*E*)-[¹¹C]ABP688-PET is presumed to be capable of capturing dynamic changes in the mGluR5-dependent neuron-astrocyte interactions subsequent to an enhanced glucose supply, although contributions of astrocytic mGluR5 to the PET-detectable radioligand binding are yet to be determined.

As exemplified by synaptic and astrocytic stimulations mediated by mGluR5, PET imaging of mGluR5 may not only be of utility as an indicator of glutamate release but could also provide information on the neuromodulatory functions of this receptor in slow and persistent components of functional fluctuations in the brain. Previous reports demonstrated the significance of mGluR5 in the regulation of stress responses,⁴⁵ circadian rhythms,⁴⁶ and feeding behaviors,⁴⁷ but these activities are associated with mGluR5 in rather confined brain areas. In contrast,

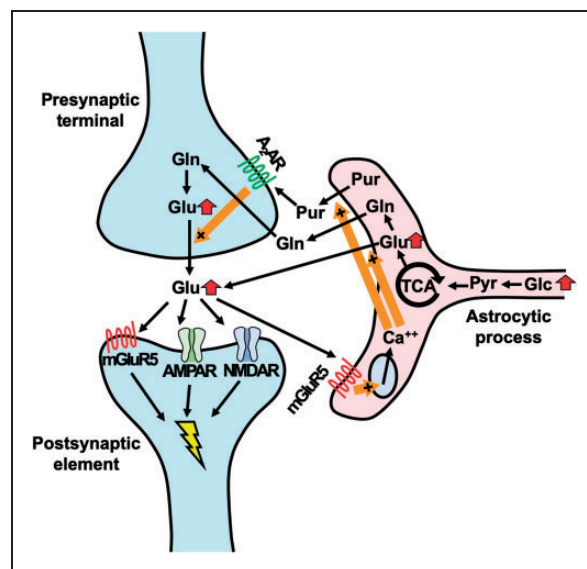


Figure 6. Schematic presentation of enhanced glutamatergic tones as a consequence of dietary glucose intakes according to the current findings. Terminals of neuronal and astrocytic processes are constituents of a tripartite synapse, in which metabolic statuses of astrocytes are mechanistically coupled with glutamatergic tones. Systemic glucose intakes could enhance the astrocytic glucose metabolism, resulting in the augmented production of glutamate in this cell type. This change triggers alternate conversions of glutamate and glutamine, leading to elevated basal excitability and synaptic glutamate release. In the meantime, glutamate can be directly released from astrocytes to synaptic and extrasynaptic spaces. In addition to postsynaptic mGluR5, astrocytic mGluR5 is stimulated by glutamate, followed by activation of the Ca⁺⁺ signals and consequent reinforcement of glutamate and purine releases from astrocytes. Presynaptic purinergic stimulations also promote the release of glutamate, forming a positive feedback loop sustaining a tonic increase of the E-I balance. Glc, glucose; Pyr, pyruvate; Glu, glutamate; Gln, glutamine; Pur, purine; A₂AR, A₂ adenosine receptor; AMPAR, AMPA receptor; NMDAR, NMDA receptor.

the current PET assays have revealed that the interactions between glutamate and mGluR5 in widespread forebrain structures are triggered by glucose intakes, conceivably giving rise to modifications of a global E-I balance. These diet-related physiological oscillations of tonic neuronal activities could become deteriorated in a diseased condition, as altered mGluR5 availability was shown to emerge in diverse neuropsychiatric disorders.^{48–52} A murine model of neurodegenerative diseases also exhibited declines of mGluR5 radioligand binding in our recent PET experiments.⁵² We therefore postulate that glucose-induced increase and fasting-induced decrease of (*E*)-[¹¹C]ABP688 binding can be dysregulated at a prodromal stage of these illnesses, which might offer biological tests to assist the clinical diagnosis.

It is also noteworthy that plasma glucose levels should be considered a confounding factor affecting the radioligand binding measures in the quantification of mGluR5 under physiological and pathological circumstances. Furthermore, results of mGluR5 PET measurements in pharmacological challenges could fluctuate as a function of systemic and cerebral glucose levels. In fact, PET studies have so far demonstrated variable effects of systemically administered glutamatergic enhancers on the binding of racemate [¹¹C]ABP688 to mGluR5.^{53–55} In addition, variations of blood and tissue glucose concentrations could influence a test-retest assessment of mGluR5 radioligand binding in a single day, as documented previously.^{17,18} In such an experimental protocol, having a meal between the two scans may cause elevated radioligand retention in the second session. We also anticipate that the associations between mGluR5 radioligand binding and glutamate levels in the brains of healthy subjects examined here would be modified under central nervous system (CNS) disorders. Interestingly, a negative correlation between these two parameters was observed in patients with major depressive disorder in a cross-sectional manner,⁵⁶ somewhat different from our present findings in healthy subjects. This finding implies disease-related alterations of E-I balances as supposed in diverse psychiatric illnesses,^{57,58} although it would be preferable to conduct these analyses while controlling for the glucose levels.

Our results showing fluctuation of the quantitative values between the two same-day scans may also have implications for various other test-retest studies in PET. While test-retest studies are often conducted on the same day, the presence or absence of food intake between the scans may potentially affect radioligand binding and may bias the validity of test-retest parameter estimations. Therefore, unless the possibilities of such confounding effects on the molecule to be

quantified can be ruled out, it would be preferable to rescan on a different day under the same condition.

Additionally, although statistically not significant, the between-group comparison in the 1st PET scan with and without food intake in our human experiments showed a trend toward slightly higher V_T values in the food-intake group, while the within-subject comparison in the 1st PET scan in our rat experiment (Experiment 1) showed a trend toward slightly higher BP_{ND} values for the scan of the non-feeding condition day. These results may suggest that (*E*)-[¹¹C]ABP688 PET could also detect inter- and intra-subject factors that affect the mGluR5 status other than food or glucose intake, which will be a subject for further investigation.

Several technical limitations should be taken into account in this study. First, the sample size in our human experiment was small, as out of the 16 subjects, only data from 11 subjects were used for full kinetic PET analysis (5 and 6 subjects for the food intake and no-food intake conditions, respectively). Therefore, although we found clear differences between the two scans, interpretation of our human experiment results should be handled with considerable caution, and future studies with larger sample sizes will be required to confirm our results. Second, we did not measure the blood levels of glucose, insulin, triglyceride, leptin, or active ghrelin in the no-food intake condition group of our human experiments. Third, to minimize confounding effects including sex differences and also because of the limited scan slot and volunteer availability, we included only male subjects in our human experiments, and accordingly only males in our rodent experiments to maintain consistency. Further studies conducting scans that include both male and female subjects will be needed to generalize our results. Fourth, as clinical MRS measurements were confined to the posterior insula, it is yet to be clarified whether glucose intakes affect the global E-I balance in the brain. To investigate glutamate concentrations in extensive brain areas and to generalize our results, it will be desirable to conduct MRS studies in regions other than the insula, and to apply multi-voxel MRS. Fifth, the PET and MRS scans in human experiments were not conducted simultaneously. To perform more precise assessments of the relationships between mGluR5 ligand binding and glutamate levels, a PET/MR system would be beneficial. Fifth, we cannot completely exclude the possibility that some of the changes in the PET and MRS signals observed in our experiments could be explained by factors other than glucose. Finally, there might be a confounding effect of physical and psychological stresses on glutamatergic activities during the PET scan. However, the inter-scan difference in mGluR5 ligand binding was not associated with stress-related

hormonal changes in plasma, which could be caused by the arterial cannulation.

In conclusion, the present work has unraveled dynamic alterations of the central glutamatergic tones and basal neuronal excitability in a close link to dietary glucose intakes. Such crosstalk among metabolic, neurochemical, and neurophysiological statuses could be pursued by *in vivo* multimodal assaying technologies and could be a point for therapeutic interventions in neuropsychiatric disorders associated with dysregulated controls of the E-I balance.

Funding

The author(s) disclosed receipt of the following financial support for the research, authorship, and/or publication of this article: This study was supported in part by Grants-in-Aid for Young Scientists (16K19790 [B] and 19K17101 to M.K., 24791352 [B] to Y.K.) from the Japan Society for the Promotion of Science. João Duarte was supported by the Knut and Alice Wallenberg Foundation. These agencies had no further role in the study design, collection, analysis or interpretation of the data, writing of the report, or in the decision to submit the paper for publication.

Acknowledgements

We thank Kazuko Suzuki and Shizuko Kawakami for their assistance as clinical coordinators, Naoto Sato for his support with MRI scans, the staff of the Department of Radiopharmaceutics Development for the radioligand synthesis and metabolite analysis, and Atsuo Waki and his team for quality assurance of the radioligand. We thank Prof. Rolf Gruetter for providing access to MRI scanners of the Centre d'Imagerie BioMédicale (CIBM) of UNIL, UNIGE, HUG, CHUV, EPFL and the Leenaards and Jeantet Foundations.

Declaration of conflicting interests

The author(s) declared no potential conflicts of interest with respect to the research, authorship, and/or publication of this article.

Authors' contribution




M.K., Y.K., and M.H. designed the study and wrote the protocol. M.K. and Y.K. managed the human experiments. M.K., Y.K., Y.Takado, C.S., H.Shimada, H.Shinotoh, K. Takahata, S.K., S.M., and K.Tagai performed the human experiments. M.T. performed the PET experiments in rats under the supervision of J.M. and M.H. J.D. performed the MRS experiments in rats. H.T. conducted two-photon calcium imaging under the supervision of J.N. and Y. Tomita. M. S. performed the experiment of the mGluR5 protein level investigation, and managed the glutamate release assay. K. K. and MR. Z. were in charge of radioligand synthesis. M.K. wrote the first draft of the manuscript. M.K. and M.H. managed the literature searches. M.K., Y.K., S.M., Y.Takado,

and J.D. undertook the analysis and interpretation of imaging data under the technical supervision of T.O., M.I., T.S., and M.H. All authors contributed to and approved the final manuscript.

Supplementary material

Supplemental material for this article is available online.

ORCID iDs

Manabu Kubota  <https://orcid.org/0000-0001-9507-1845>
Yasuyuki Kimura  <https://orcid.org/0000-0002-7927-9483>
Takayuki Obata  <https://orcid.org/0000-0001-7678-5033>

References

- Seamans JK, Nogueira L and Lavin A. Synaptic basis of persistent activity in prefrontal cortex *in vivo* and in organotypic cultures. *Cereb Cortex* 2003; 13: 1242–1250.
- Nasca C, Bigio B, Zelli D, et al. Mind the gap: glucocorticoids modulate hippocampal glutamate tone underlying individual differences in stress susceptibility. *Mol Psychiatry* 2015; 20: 755–763.
- Pava MJ, den Hartog CR, Blanco-Centurion C, et al. Endocannabinoid modulation of cortical up-states and NREM sleep. *PLoS One* 2014; 9: e88672.
- Sonnay S, Gruetter R and Duarte JMN. How energy metabolism supports cerebral function: insights from ¹³C magnetic resonance studies *in vivo*. *Front Neurosci* 2017; 11: 288.
- Yu AC, Drejer J, Hertz L, et al. Pyruvate carboxylase activity in primary cultures of astrocytes and neurons. *J Neurochem* 1983; 41: 1484–1487.
- Norenberg MD and Martinez-Hernandez A. Fine structural localization of glutamine synthetase in astrocytes of rat brain. *Brain Res* 1979; 161: 303–310.
- Kvamme E, Torgner IA and Roberg B. Kinetics and localization of brain phosphate activated glutaminase. *J Neurosci Res* 2001; 66: 951–958.
- Ottersen OP, Zhang N and Walberg F. Metabolic compartmentation of glutamate and glutamine: morphological evidence obtained by quantitative immunocytochemistry in rat cerebellum. *Neuroscience* 1992; 46: 519–534.
- Klement J, Hubold C, Cords H, et al. High-calorie glucose-rich food attenuates neuroglycopenic symptoms in patients with Addison's disease. *J Clin Endocrinol Metab* 2010; 95: 522–528.
- Wilson M, Andronesi O, Barker PB, et al. Methodological consensus on clinical proton MRS of the brain: review and recommendations. *Magn Reson Med* 2019; 82: 527–550.
- Oz G, Alger JR, Barker PB, et al. Clinical proton MR spectroscopy in central nervous system disorders. *Radiology* 2014; 270: 658–679.
- Duarte JM, Lei H, Mlynarik V, et al. The neurochemical profile quantified by *in vivo* ¹H NMR spectroscopy. *Neuroimage* 2012; 61: 342–362.

13. Takado Y, Takuwa H, Sampei K, et al. MRS-measured glutamate versus GABA reflects excitatory versus inhibitory neural activities in awake mice. *bioRxiv* 2020. DOI: 10.1101/2020.10.25.353888.
14. Hong J, Lu S, Xu R, et al. [*carbonyl*- ^{11}C]4-Fluoro-*N*-methyl-*N*-(4-(6-(methylamino)pyrimidin-4-yl)thiazol-2-yl) benzamide ([^{11}C]FIMX) is an effective radioligand for PET imaging of metabotropic glutamate receptor 1 (mGluR1) in monkey brain. *Nucl Med Biol* 2015; 42: 967–974.
15. Ametamey SM, Kessler LJ, Honer M, et al. Radiosynthesis and preclinical evaluation of ^{11}C -ABP688 as a probe for imaging the metabotropic glutamate receptor subtype 5. *J Nucl Med* 2006; 47: 698–705.
16. Patel S, Hamill TG, Connolly B, et al. Species differences in mGluR5 binding sites in mammalian central nervous system determined using *in vitro* binding with [^{18}F]FPEB. *Nucl Med Biol* 2007; 34: 1009–1017.
17. DeLorenzo C, Kumar JS, Mann JJ, et al. *In vivo* variation in metabotropic glutamate receptor subtype 5 binding using positron emission tomography and [^{11}C]ABP688. *J Cereb Blood Flow Metab* 2011; 31: 2169–2180.
18. DeLorenzo C, Gallezot JD, Gardus J, et al. *In vivo* variation in same-day estimates of metabotropic glutamate receptor subtype 5 binding using [^{11}C]ABP688 and [^{18}F]FPEB. *J Cereb Blood Flow Metab* 2017; 37: 2716–2727.
19. Kawamura K, Yamasaki T, Kumata K, et al. Binding potential of (*E*)-[^{11}C]ABP688 to metabotropic glutamate receptor subtype 5 is decreased by the inclusion of its ^{11}C -labelled Z-isomer. *Nucl Med Biol* 2014; 41: 17–23.
20. Logan J, Fowler JS, Volkow ND, et al. Graphical analysis of reversible radioligand binding from time-activity measurements applied to [*N*- ^{11}C -methyl]-(-)-cocaine PET studies in human subjects. *J Cereb Blood Flow Metab* 1990; 10: 740–747.
21. Hannestad J, Subramanyam K, Dellagioia N, et al. Glucose metabolism in the insula and cingulate is affected by systemic inflammation in humans. *J Nucl Med* 2012; 53: 601–607.
22. Allport LE, Butcher KS, Baird TA, et al. Insular cortical ischemia is independently associated with acute stress hyperglycemia. *Stroke* 2004; 35: 1886–1891.
23. Wright H, Li X, Fallon NB, et al. Differential effects of hunger and satiety on insular cortex and hypothalamic functional connectivity. *Eur J Neurosci* 2016; 43: 1181–1189.
24. Tang DW, Fellows LK, Small DM, et al. Food and drug cues activate similar brain regions: a meta-analysis of functional MRI studies. *Physiol Behav* 2012; 106: 317–324.
25. Craig AD. How do you feel? Interoception: the sense of the physiological condition of the body. *Nat Rev Neurosci* 2002; 3: 655–666.
26. Ogg RJ, Kingsley PB and Taylor JS. WET, a T1- and B1-insensitive water-suppression method for *in vivo* localized ^1H NMR spectroscopy. *J Magn Reson B* 1994; 104: 1–10.
27. Tomiyasu M, Aida N, Endo M, et al. Neonatal brain metabolite concentrations: an *in vivo* magnetic resonance spectroscopy study with a clinical MR system at 3 Tesla. *PLoS One* 2013; 8: e82746.
28. Berger GE, Wood SJ, Wellard RM, et al. Ethyl-eicosa-pentaenoic acid in first-episode psychosis. A ^1H -MRS study. *Neuropsychopharmacology* 2008; 33: 2467–2473.
29. Destrieux C, Fischl B, Dale A, et al. Automatic parcellation of human cortical gyri and sulci using standard anatomical nomenclature. *Neuroimage* 2010; 53: 1–15.
30. Duarte JM and Gruetter R. Characterization of cerebral glucose dynamics *in vivo* with a four-state conformational model of transport at the blood-brain barrier. *J Neurochem* 2012; 121: 396–406.
31. Mlynarik V, Gambarota G, Frenkel H, et al. Localized short-echo-time proton MR spectroscopy with full signal-intensity acquisition. *Magn Reson Med* 2006; 56: 965–970.
32. Chen TW, Wardill TJ, Sun Y, et al. Ultrasensitive fluorescent proteins for imaging neuronal activity. *Nature* 2013; 499: 295–300.
33. Shimojo M, Ono M, Takuwa H, et al. Genetically targeted reporter imaging of deep neuronal network in the mammalian brain. *bioRxiv* 2020. DOI: 10.1101/2020.04.08.032870.
34. Tomita Y, Kubis N, Calando Y, et al. Long-term *in vivo* investigation of mouse cerebral microcirculation by fluorescence confocal microscopy in the area of focal ischemia. *J Cereb Blood Flow Metab* 2005; 25: 858–867.
35. Takuwa H, Autio J, Nakayama H, et al. Reproducibility and variance of a stimulation-induced hemodynamic response in barrel cortex of awake behaving mice. *Brain Res* 2011; 1369: 103–111.
36. Carson RE, Breier A, de Bartolomeis A, et al. Quantification of amphetamine-induced changes in [^{11}C]raclopride binding with continuous infusion. *J Cereb Blood Flow Metab* 1997; 17: 437–447.
37. Laruelle M. Imaging synaptic neurotransmission with *in vivo* binding competition techniques: a critical review. *J Cereb Blood Flow Metab* 2000; 20: 423–451.
38. Volkow ND, Wang GJ, Fowler JS, et al. Imaging endogenous dopamine competition with [^{11}C]raclopride in the human brain. *Synapse* 1994; 16: 255–262.
39. Chugani DC, Ackermann RF and Phelps ME. *In vivo* [^3H]spiperone binding: evidence for accumulation in corpus striatum by agonist-mediated receptor internalization. *J Cereb Blood Flow Metab* 1988; 8: 291–303.
40. Hall H, Wedel I, Halldin C, et al. Comparison of the *in vitro* receptor binding properties of *N*-[^3H]methylspiperone and [^3H]raclopride to rat and human brain membranes. *J Neurochem* 1990; 55: 2048–2057.
41. Guo N, Guo W, Kralikova M, et al. Impact of D2 receptor internalization on binding affinity of neuroimaging radiotracers. *Neuropsychopharmacology* 2010; 35: 806–817.
42. Sun W, Ginovart N, Ko F, et al. *In vivo* evidence for dopamine-mediated internalization of D₂-receptors after amphetamine: differential findings with [^3H]raclopride versus [^3H]spiperone. *Mol Pharmacol* 2003; 63: 456–462.

43. Malarkey EB and Parpura V. Mechanisms of glutamate release from astrocytes. *Neurochem Int* 2008; 52: 142–154.
44. Panatier A and Robitaille R. Astrocytic mGluR5 and the tripartite synapse. *Neuroscience* 2016; 323: 29–34.
45. Peterlik D, Flor PJ and Uschold-Schmidt N. The emerging role of metabotropic glutamate receptors in the pathophysiology of chronic stress-related disorders. *Curr Neuroparmacol* 2016; 14: 514–539.
46. Elmenhorst D, Mertens K, Kroll T, et al. Circadian variation of metabotropic glutamate receptor 5 availability in the rat brain. *J Sleep Res* 2016; 25: 754–761.
47. Charles JR, Duva MA, Ramirez GJ, et al. Activation of lateral hypothalamic mGlu1 and mGlu5 receptors elicits feeding in rats. *Neuropharmacology* 2014; 79: 59–65.
48. Holmes SE, Girgenti MJ, Davis MT, et al. Altered metabotropic glutamate receptor 5 markers in PTSD: in vivo and postmortem evidence. *Proc Natl Acad Sci U S A* 2017; 114: 8390–8395.
49. Mihov Y, Treyer V, Akkus F, et al. Metabotropic glutamate receptor 5 in bulimia nervosa. *Sci Rep* 2020; 10: 6374.
50. Lohith TG, Osterweil EK, Fujita M, et al. Is metabotropic glutamate receptor 5 upregulated in prefrontal cortex in fragile X syndrome? *Mol Autism* 2013; 4: 15.
51. Leuzy A, Zimmer ER, Dubois J, et al. In vivo characterization of metabotropic glutamate receptor type 5 abnormalities in behavioral variant FTD. *Brain Struct Funct* 2016; 221: 1387–1402.
52. Shimojo M, Takuwa H, Takado Y, et al. Selective disruption of inhibitory synapses leading to neuronal hyperexcitability at an early stage of tau pathogenesis in a mouse model. *J Neurosci* 2020; 40: 3491–3501.
53. Miyake N, Skinbjerg M, Easwaramoorthy B, et al. Imaging changes in glutamate transmission in vivo with the metabotropic glutamate receptor 5 tracer [¹¹C] ABP688 and N-acetylcysteine challenge. *Biol Psychiatry* 2011; 69: 822–824.
54. DeLorenzo C, DellaGioia N, Bloch M, et al. In vivo ketamine-induced changes in [¹¹C]ABP688 binding to metabotropic glutamate receptor subtype 5. *Biol Psychiatry* 2015; 77: 266–275.
55. Sandiego CM, Nabulsi N, Lin SF, et al. Studies of the metabotropic glutamate receptor 5 radioligand [¹¹C] ABP688 with N-acetylcysteine challenge in rhesus monkeys. *Synapse* 2013; 67: 489–501.
56. Abdallah CG, Hannestad J, Mason GF, et al. Metabotropic glutamate receptor 5 and glutamate involvement in major depressive disorder: a multimodal imaging study. *Biol Psychiatry Cogn Neurosci Neuroimaging* 2017; 2: 449–456.
57. Ferguson BR and Gao WJ. PV Interneurons: critical regulators of E/I balance for prefrontal cortex-dependent behavior and psychiatric disorders. *Front Neural Circuits* 2018; 12: 37.
58. Delevich K, Jaaro-Peled H, Penzo M, et al. Parvalbumin interneuron dysfunction in a thalamo-prefrontal cortical circuit in disc1 locus impairment mice. *eNeuro* 2020; 7. doi: 10.1523/ENEURO.0496-19.2020